PNAS RESEARCH ARTICLE | GENETICS

Discrete roles of Ir76b ionotropic coreceptor impact olfaction, blood feeding, and mating in the malaria vector mosquito *Anopheles coluzzii*

Zi Ye[a,1], Feng Liu[a,1], Huahua Sun[a], Stephen T. Ferguson[a], Adam Baker[a], Samuel A. Ochieng[a], and Laurence J. Zwiebel[a,2]

Edited by John Hildebrand, The University of Arizona, Tucson, AZ; received July 5, 2021; accepted April 13, 2022

Anopheline mosquitoes rely on their highly sensitive chemosensory apparatus to detect diverse chemical stimuli that drive the host-seeking and blood-feeding behaviors required to vector pathogens for malaria and other diseases. This process incorporates a variety of chemosensory receptors and transduction pathways. We used advanced in vivo gene-editing and -labeling approaches to localize and functionally characterize the ionotropic coreceptor *AcIr76b* in the malaria mosquito *Anopheles coluzzii*, where it impacts both olfactory and gustatory systems. *AcIr76b* has a broad expression pattern in female adult antennal grooved pegs, coeloconic sensilla, and T1 and T2 sensilla on the labellum, stylets, and tarsi, as well as the larval sensory peg. *AcIr76b* is colocalized with the Orco odorant receptor (OR) coreceptor in a subset of cells across the female antennae and labella. In contrast to *Orco* and *Ir8a*, chemosensory coreceptors that appear essential for the activity of their respective sets of chemosensory neurons in mosquitoes, $AcIr76b^{-/-}$ mutants maintain wild-type peripheral responses to volatile amines on the adult palps, labellum, and larval sensory cone. Interestingly, $AcIr76b^{-/-}$ mutants display significantly increased responses to amines in antennal grooved peg sensilla, while coeloconic sensilla reveal significant deficits in responses to several acids and amines. Behaviorally, *AcIr76b* mutants manifest significantly female-specific insemination deficits, and although $AcIr76b^{-/-}$ mutant females can locate, alight on, and probe artificial blood hosts, they are incapable of blood feeding successfully. Taken together, our findings reveal a multidimensional functionality of Ir76b in anopheline olfactory and gustatory pathways that directly impacts the vectorial capacity of these mosquitoes.

Anopheles coluzzii | olfaction | ionotropic receptor | electrophysiology | blood feeding

Significance

Chemosensory systems play crucial roles across mosquito life cycles, with underlying molecular receptors often forming functional complexes that require cognate coreceptors. To better understand chemosensory pathways in the malaria vector mosquito *Anopheles coluzzii*, gene editing were used to localize and functionally characterize the ionotropic receptor coreceptor *AcIr76b*. Expression of *AcIr76b* was observed in antennal grooved pegs, coeloconic sensilla, and other accessory olfactory appendages. When *AcIr76b* was inactivated, mutant mosquitoes displayed altered neuronal responses to amines.. Beyond olfactory phenotypes, *AcIr76b* mutants display significantly impaired mating and blood feeding capabilities. Our data reveal discrete roles of *AcIr76b* across chemosensory pathways, suggesting ionotropic pathways as targets for the design of vector control strategies.

The malaria mosquito *Anopheles coluzzii* [recently renamed from the "M" form of *Anopheles gambiae* (1)] is a major vector of human malaria pathogens in sub-Saharan Africa that are transmitted during blood feeding by adult females (2). Anophelines and other mosquitoes locate blood-meal hosts through detection of a variety of environmental and host-derived cues, among which olfactory signals have great significance at both long and short range (3, 4). On the head of adult mosquitoes, the primary olfactory appendages include the antennae, maxillary palps, and labella, which are covered by a range of hairlike protrusions known as sensilla (5–8). One or more bipolar olfactory sensory neurons (OSNs) innervate a typical chemosensory sensillum where their dendrites extend apically and are bathed within an aqueous lymph (8, 9). Three large gene families encode the distinct molecular receptors that underlie olfaction in mosquitoes and other insects; these include odorant receptors (ORs), ionotropic receptors (IRs), and gustatory receptors (GRs) (4). These receptors are expressed on the dendritic membranes of diverse sets of chemosensory neurons, where they generate action potentials in response to a broad spectrum of chemical stimuli (5, 7, 10–13). Three major morphological types of olfactory sensilla are present on the mosquito antennae: trichoid, basiconic (also known as grooved peg), and coeloconic sensilla (9, 14). In *An. coluzzii*, while there is a range of functional variations within each type of sensillum, trichoid sensilla generally respond to a broad spectrum of odorants, while both grooved pegs and coeloconic sensilla appear to be more narrowly tuned to both amines and acids (6, 15, 16).

While molecularly unrelated, mosquito ORs and IRs are both ligand-gated heteromeric channels composed of tuning subunits along with one or more highly conserved coreceptor subunits (17–20). The tuning subunit is responsible for the specificity of the receptor, while the coreceptor maintains the structural integrality and is crucial for receptor function (19–21). Knockout (null) mutants of the odorant receptor coreceptor (Orco) in *Aedes aegypti* and *An. coluzzii* result in a dramatic decrease in sensitivity to a variety of human and other odorants; however, importantly, humans remain attractive to host-seeking

The authors declare no competing interest.

This article is a PNAS Direct Submission.

Copyright © 2022 the Author(s). Published by PNAS. This article is distributed under Creative Commons Attribution-NonCommercial-NoDerivatives License 4.0 (CC BY-NC-ND).

[1]Z.Y. and F.L. contributed equally to this work.

[2]To whom correspondence may be addressed. Email: l.zwiebel@vanderbilt.edu.

This article contains supporting information online at http://www.pnas.org/lookup/suppl/doi:10.1073/pnas.2112385119/-/DCSupplemental.

Published June 1, 2022.

Orco$^{-/-}$ mutants, highlighting the involvement of other odorant signaling pathways and sensory modalities (21, 22).

In *Drosophila*, antennal IRs are primarily expressed in the coeloconic sensilla (18). Unlike ORs, which rely on a single coreceptor (Orco), three IRs—Ir8a, Ir25a, and Ir76b—function as IR coreceptors (18, 19). Interestingly, each *Drosophila melanogaster* ionotropic receptor (DmIR) coreceptor is associated with distinct odor preferences; *DmIr8a* is critical for acid sensitivity, whereas *DmIr25a* and *DmIr76b* are both responsible for amine detection (18, 23, 24). In addition to olfactory function, Ir76b and Ir25a are also involved in other sensory modalities and pathways. In *Drosophila*, DmIr76b has been found to be involved in gustatory responses to salt and amino acids (25, 26), and DmIr25a acts in both thermosensation and hydrosensation (27, 28). Furthermore, while *DmIr25a* and *DmIr76b* are both coexpressed with DmIr92a acting as a *Drosophila* ammonia/amine receptor, DmIr92a is able to function independently of either of these coreceptors (24, 29).

Recently, several studies focusing on mosquito IRs have revealed that the homologs to *Drosophila* IR coreceptors similarly regulate a range of Orco-independent sensing pathways. In the arbovirus vector *Ae. aegypti*, *AeIr8a* null mutants lost the neuronal and behavioral responses to acids (30). In *An. coluzzii* larvae, all three IR coreceptors are expressed on the larval antennae, and RNA interference (RNAi) knockdown of *AcIr76b* specifically impacts larval responses to butylamine (31). In adults, *AcIr76b* is highly expressed in antennal neurons that do not express ORs (11); in *Xenopus* oocytes, it drives responses to several amines when coexpressed with *AcIr25a* and either *AcIr41a* or *AcIr41c* (11).

To examine the roles and relevance of Ir76b in the olfactory system of *An. coluzzii*, we utilized CRISPR-Cas9–mediated gene editing to establish an *AcIr76b-QF2* driver and *AcIr76b* null mutant lines. Localization studies using the driver within a binary Q system (32) reveal that *AcIr76b* is robustly expressed in antennal grooved pegs, coeloconic sensilla, labella, stylets, and tarsi of adult females, as well as in the larval antennae where it specifically innervates the sensory peg. Surprisingly, adult female *AcIr76b*$^{-/-}$ mosquitoes display significantly increased antennal responses to several amines, whereas peripheral responses to acid stimuli are unaffected. Behaviorally, *AcIr76b* mutant females display severe mating deficits and, interestingly, have acutely lost the ability to blood feed successfully. These studies demonstrate that *AcIr76b* acts in both olfactory and gustatory systems of *An. coluzzii*, where it impacts the reproductive fitness and ultimately the vectorial capacity of this globally important mosquito.

Materials and Methods

Mosquito Rearing. *An. coluzzii* (SUA 2La/2La), previously known as *Anopheles gambiae sensu stricto* "M-form" (1), originating from Suakoko, Liberia, was obtained through BEI Resources, National Institute of Allergy and Infectious Diseases (NIAID), NIH: *Anopheles gambiae*, Strain SUA2La, Eggs, MRA-765, contributed by Alessandra della Torre at University of Rome "La Sapienza", Rome, Italy. Mosquito lines were reared at 27 °C, 75% humidity under a 12-h light/12-h dark photoperiod and supplied with 10% sucrose water in the Vanderbilt University Insectary (33, 34). For stock propagation, 5- to 7-d-old mated females were blood fed for 30 to 45 min using a membrane feeding system (Hemotek) filled with defibrinated sheep blood purchased from Hemostat Laboratories. Mosquito larvae were reared in distilled water at 27 °C under the standard 12-h light/12-h dark cycle, with ∼300 larvae per rearing pan in 1 L H_2O. The larval food was made from 0.12 g/mL Kaytee Koi's Choice premium fish food plus 0.06 g/mL yeast in distilled water and subsequently incubated at 4 °C overnight for fermentation. For first and second instar larvae, 0.08 mL larval food was added into the water every 24 h. The *An. coluzzii* effector line (QUAS-mCD8:GFP) was a generous gift from the laboratory of C. Potter at The Johns Hopkins University School of Medicine, Baltimore, MD (available via BEI Resources, NIAID, NIH: *An. coluzzii*, Strain QUAS-CD8:GFP, Eggs, MRA-1301).

Mosquito Mutagenesis CRISPR-Cas9 gene editing in *An. coluzzii* was carried out as previously described (35). The CRISPR gene-targeting vector was the generous gift from the laboratory of Andrea Crisanti at Imperial College London, London, UK (36). The single-guide RNA (sgRNA) sequence was designed by CHOPCHOP (37) to target the first exon of *AcIr76b* gene (ACOM032257). The complimentary oligos (Ir76b_gRNA_F/Ir76b_gRNA_R; *SI Appendix*, Table S1) were artificially synthesized (Integrated DNA Technologies) and subcloned into the CRISPR vector by Golden Gate cloning (New England Biolabs). The homologous templates were constructed based on the pHD-DsRed vector (Kate O'Connor-Giles, Brown University, Providence, RI; Addgene plasmid #51434; n2t.net/addgene:51434; RRID:Addgene 51434), where the 2-kb homologous arms extending either direction from the double-strand break (DSB) site were PCR amplified with the customized oligonucleotide primers: Ir76b_AarI_F/Ir76b_AarI_R; Ir76b_SapI_F/Ir76b_SapI_R (*SI Appendix*, Table S1) and sequentially inserted into the AarI/SapI restriction sites on the vector.

The microinjection protocol followed a previous study (16, 38). In brief, newly laid (∼1-h-old) embryos of the wild-type *An. coluzzii* were immediately collected and aligned on a filter paper moistened with 25 mM sodium chloride solution. All the embryos were fixed on a coverslip with double-sided tape, and a drop of halocarbon oil 27 was applied to cover the embryos. The coverslip was further fixed on a slide under a Zeiss Axiovert 35 microscope with a 40× objective. The microinjection was performed using Eppendorf FemtoJet 5247 and quartz needles (Sutter Instrument). The gene-targeting vector and the homologous template were coinjected at 300 ng/μL each. Injected embryos were subsequently placed in deionized water with artificial sea salt (0.3 g/L) and thereafter reared under normal Vanderbilt University insectary conditions.

First-generation (G0) injected adults were separated based on sex and crossed to 5× wild-type sex counterparts. Their offspring (F1) were screened for DsRed-derived red eye fluorescence. Red-eyed F1 males were individually crossed to 5× wild-type females to establish a stable mutant line. DNA extraction was performed using DNeasy Blood and Tissue kits following the manufacturer's instruction (Qiagen), and genomic DNA was used as templates for PCR analyses of all individuals (after mating) to validate the fluorescence marker insertion using primers that cover DSB sites (Ir76b_F/Ir76b_R; *SI Appendix*, Table S1). Salient PCR products were sequenced to confirm the accuracy of the genomic insertion. The heterozygous mutant lines were thereafter back-crossed to the wild-type *An. coluzzii* for at least five generations before putative homozygous individuals were manually screened for DsRed-derived red eye fluorescence intensity. Putative homozygotic mutant individuals were mated to each other before being killed for genomic DNA extraction and PCR analyses (as above) to confirm their homozygosity.

To generate the *AcIr76b-QF2* driver line for Q system, *T2A-QF2-3xP3-DsRed* element was inserted into the *Ir76b* coding region through CRISPR-mediated homologous recombination. DSB was induced using the CRISPR gene-targeting vector described above. The homologous template that contains *T2A-QF2-3xP3-DsRed* element, which was amplified from the ppk301-T2A-QF2 HDR plasmid ((39); Leslie Vosshall, Rockefeller University, New York, NY; Addgene plasmid# 130667; n2t.net/addgene:130667; RRID:Addgene_130667), flanked by ∼2-kb homologous arms, was constructed using NEBuilder HiFi DNA Assembly kit (NEB) (Ir76b_LArm_F/Ir76b_LArm_R; Ir76b_RArm_F/Ir76b_RArm_R; Ir76b_T2A_F/Ir76b_T2A_R; *SI Appendix*, Table S1). From the left homologous arm immediately preceding the *T2A*, 2 bp were removed to keep the *T2A* sequence in-frame. Red-eyed F1 mosquitoes were backcrossed for three generations and then crossed to the effector line to acquire progeny for Ir76b localization studies.

Whole-Mount Imaging. Larval offspring resulting from crosses between the heterozygous *AcIr76b-QF2* driver line and the *QUAS-mCD8:GFP* effector were screened for eye-specific expression of DsRed. Larval head appendages as well as whole adult antennae, maxillary palps, proboscis, and tarsi from 4- to 6-d-old adult females were dissected into 4% formaldehyde in PBST (0.1% Triton X-100 in phosphate-buffered saline) and fixed on ice for 30 min in the case of the tarsi and larval head appendages or at 4 °C for 24 h for adult antennae. Samples were thereafter washed 3X in PBST for 10 min each and directly transferred onto Superfrost plus slides (VWR Scientific) and mounted in Vectashield fluorescent medium (Vector Laboratories). Confocal microscopy images at 1024 × 1024

pixel resolution were collected with an Olympus FV-1000 instrument equipped with a 100× oil objective at the Vanderbilt University Cell Imaging Shared Resource Core. Laser wavelengths of 405 nm, 488 nm, and 543 nm were used to detect DAPI, green fluorescent protein (GFP), and Cy3, respectively.

Immunohistochemistry. Antibody staining was performed as previously described (10, 16). Antennae, labella, and maxillary palps were dissected into 4% formaldehyde in PBST and fixed on ice for 30 min. Samples were washed 3× in PBST for 10 min each and then embedded in Tissue Freezing Medium (General Data Company Inc.). Cryosections were obtained at −20 °C using a CM1900 cryostat (Leica Microsystems). Samples were sectioned at ∼10 μm and transferred onto Superfrost plus slides (VWR Scientific). Slides were air-dried at room temperature (RT) for 30 min and fixed in 4% formaldehyde in PBST for 10 min, followed by 3× rinsing in PBST for 10 min each. Thereafter, 5% normal goat serum (Sigma-Aldrich) in PBST was applied, and the slides were blocked in the dark at RT for 1 h in HybriWell sealing chambers (Grace Bio-Labs). Primary antibody Rabbit α-Orco was diluted 1:500 in 5% normal goat serum in PBST and applied on the slides and incubated overnight at 4 °C.

After primary antibody staining, slides were washed 3× in PBST for 10 min each and stained with secondary antibody Goat α-Rabbit-Cy3 (Jackson ImmunoResearch) 1:500 in 5% normal goat serum PBST for 2 h at RT and then rinsed 3×. Nuclei were stained with 300 nM DAPI (Invitrogen) at RT for 10 min. Slides were briefly washed and mounted in Vectashield medium (Vector Laboratories). Whole-mount samples were dissected into 4% formaldehyde in PBST and fixed on ice for 30 min. After 3× washing in PBST for 10 min each, the samples were transferred onto slides and mounted in Vectashield medium (Vector Laboratories). Confocal microscopy images were collected as detailed above for the whole mounts.

Transcuticular Electrophysiology/Mass Measurements. Electroantennogram (EAG) and electrolabellogram (ELG) recordings were conducted as previously detailed, with modifications (7, 34). Female mosquitoes (4 to 10 d after eclosion) with legs and wings removed were fixed on glass slides using double-sided tape. The last segment of antenna with the tip partially cut was subsequently connected to a recording glass electrode filled with Ringer solution [96 mM NaCl, 2 mM KCl, 1 mM $MgCl_2$, 1 mM $CaCl_2$, and 5 mM 4-(2-hydroxyethyl)-1-piperazineethanesulfonic acid (Hepes), pH 7.5], to which a silver wire was in contact to complete the circuit with another glass reference electrode similarly connected into the compound eye of the female. The antennal preparation was continuously exposed to humidified, charcoal-filtered airflow (1.84 L/min) transferred through a borosilicate glass tube (inner diameter, 0.8 cm) using a stimulus controller (Syntech), and the open end of the glass tube was located 1 cm from the antennal preparation. All chemicals were diluted to 10^{-1} (vol/vol) working solutions in paraffin oil except for lactic acid, acetic acid, ammonia, and dimethylamine, which were diluted in double-distilled water (ddH_2O). Ten-microliter aliquots of test or control stimuli were transferred onto filter paper strips (3 × 50 mm), which were then placed inside the Pasteur pipette. Odors were delivered to the antennal preparation for 500 ms through a hole placed on the side of the glass tube located 10 cm from the open end of the tube (1.08 L/min), and the stimulus odor was mixed with continuous airflow through the hole. A charcoal-filtered airflow (0.76 L/min) was delivered from another valve through a blank pipette into the glass tube at the same distance from the preparation in order to minimize changes in flow rate during odor stimulation. For dose–response experiments, the working solutions were further diluted to 10^{-2}, 10^{-3}, and 10^{-4} (vol/vol). Stimulations were applied, always proceeding from the lowest concentration (10^{-4}) to the highest (10^{-1}). Control stimuli (paraffin oil and water) were applied at the beginning and end of each concentration. The resulting signals were amplified 10× and imported into a Windows PC via an intelligent data acquisition controller (IDAC, Syntech) interface box. These recordings were analyzed using EAG software (EAG Version 2.7, Syntech) such that stimulus-evoked response amplitudes were normalized by dividing the response amplitude of control (solvent alone) responses. Subsequent to each round of electrophysiological assays, the carcasses from individual mosquitoes were weighed using an XSR Analytical Balance (Mettler Toledo) to obtain comparative mass measurements.

Single-Sensillum Recording (SSR). SSRs were carried out as previously described (40, 41) with minor modifications. Female adult mosquitoes (4 to 10 d after eclosion) were mounted on a microscope slide (76 × 26 mm). Using double-sided tape, the antennae were fixed to a coverslip resting on a small bead of dental wax to facilitate manipulation, and the coverslip was placed at ∼30 degrees to the mosquito head. Once mounted, the specimen was placed under an Olympus BX51WI microscope, and the antennae were viewed at high magnification (1,000×). Recordings were carried out using two tungsten microelectrodes freshly sharpened in 10% KNO_2 at 10V. The grounded reference electrode was inserted into the compound eye of the mosquito using a WPI micromanipulator, and the recording electrode was connected to the preamplifier (Syntech Universal AC/DC 10×, Syntech) and inserted into the shaft of the olfactory sensillum to complete the electrical circuit to extracellularly record OSN potentials (42). Controlled manipulation of the recording electrode was performed using a Burleigh micromanipulator (Model PCS6000). The preamplifier was connected to an analog-to-digital signal converter (IDAC-4, Syntech), which in turn was connected to a Windows PC computer for signal recording, analysis, and visualization. Spike analyses were conducted with Auto Spike v. 3.7 (Syntech), where AC signals (action potentials or spikes) were bandpass filtered between 100 and 10,000 Hz and DC signals (receptor potentials/sensillum potentials) were analyzed with a high filter of 3 kHz. A low-pass filter was set for DC. Background (spontaneous) neuronal activity was quantified using the Auto-Spike software for 1 s/sensillum prior to any odor stimulation and averaged for at least 10 sensilla of the same morphological type. Signals were recorded for 10 s, starting 1 s before stimulation, and the action potential spikes were counted offline over a 500-ms period before and after stimulation. Spike rates observed during the 500-ms stimulation were subtracted from the spontaneous (background) spike activity observed in the preceding 500 ms, and counts were recorded in units of spikes/s. Poststimulus "OFF" responses were calculated by subtracting the prestimulus background activities from the spike counts in the 1 s immediately following the stimulus application. Responses of odorants were always normalized by subtracting the solvent responses.

All chemicals were diluted to 10^{-2} (vol/vol) working solutions in paraffin oil except for lactic acid, acetic acid, and dimethylamine, which were diluted in ddH_2O. For each chemical, a 10-μL aliquot was applied onto a filter paper (3 × 50 mm), which was then inserted into a Pasteur pipette to create the stimulus cartridge. A sample containing the solvent (paraffin oil or water) alone served as the control. The airflow was maintained at a constant 20 mL/s throughout the experiment. Purified and humidified air was delivered to the preparation through a glass tube (10-mm inner diameter) perforated by a small hole 10 cm away from the end into which the tip of the Pasteur pipette could be inserted. The stimulus was delivered to the sensilla by inserting the tip of the stimulus cartridge into this hole and diverting a portion of the air stream (0.5 L/min) to flow through the stimulus cartridge for 500 ms using a stimulus controller (Syntech). The distance between the end of the glass tube and the antennae was ≤1 cm.

Mating Bioassay. Newly emerged wild-type females and males were segregated on day 1 to ensure no mating occurred. Three-day-old females (15/bucket) and males (10/bucket) were then placed in a rearing bucket and allowed to mate freely for 5 d. All surviving females were then collected, and their spermathecae were dissected under a compound microscope. The spermathecae were then placed in the buffer (145 mM NaCl, 4 mM KCl, 1 mM $MgCl_2$, 1.3 mM $CaCl_2$, 5 mM D-glucose, and 10 mM Hepes) (43) with 300 nM DAPI, and a coverslip was used to gently press and break the spermathecae to release the sperm. As in previous studies (15), the spermathecae were examined under the 1,000× compound microscope to assess the insemination status. The insemination rate was calculated by dividing the number of inseminated females by the total number of females in each bucket.

Blood-Feeding Dioassays. Initial blood-feeding bioassays were carried out with 6- to 8-d-old wild-type and *Aclr76b* mutant females between ZT11 and ZT12, during which *An. coluzzii* was shown to be behaviorally active. Mosquitoes were starved, with only water access for 24 h prior to the bioassay. Defibrinated sheep blood was stored at 4 °C and used within 2 wk of purchasing (Hemostat Laboratories). Human foot odorants were provided as cloth strips cut from cotton socks that had been continually worn for 3 to 5 d by a 30-y-old male volunteer and thereafter incubated overnight at 37 °C in a sealed Ziploc plastic bag (SC Johnson). The acquisition and use of human foot odorants in these studies was reviewed by Vanderbilt's Institutional Review Board (IRB), which deemed them exempt from requiring human subject research approval. For each replicate, 25 to 30 female mosquitoes were released into a 32-oz container, the top of which was covered with a net through which the mosquito proboscises could

penetrate to feed but not to escape. A single membrane feeder (Hemotek) that heated the blood to 37 °C was then placed on the net. A mini camera (GoPro) was set at the bottom of the container to record the landing activity of mosquitoes. A human volunteer gently exhaled into the container for 5 s to activate the mosquitoes with CO_2 for blood feeding. The mosquitoes were allowed to feed freely for 25 min and then were immediately anesthetized at −20 °C to assess the number with blood-engorged abdomens, indicative of successful blood feeding. The assay containers and videos were also analyzed post hoc by volunteers blinded to the experimental genotypes, who manually counted both blood-engorged mosquitoes and the number of landings onto the feeder during the assay. The total landing count was divided by the total mosquito number in each assay to calculate the landing number per mosquito. Extended blood-feeding assays for wild-type and mixed populations of *AcIr76b* hetero/homozygotic mutants were similarly conducted for 120 min (2 h) using both sheep and human blood obtained from a donor volunteer through the Vanderbilt Center for Immunobiology (VCI). The donor provided informed consent, and this sample was provided by the VCI under IRB approval. Blood samples were de-identified prior to use in our study. Human odorants were obtained from the well-worn/incubated cotton socks of a 64-y-old male volunteer (as before, the acquisition and use of human foot odorants was reviewed and deemed exempt from IRB approval for human subject research). Here, mosquitoes were allowed to feed freely for full duration of the assay and then were immediately anesthetized at −20 °C to assess the number with blood-engorged abdomens, indicative of successful blood feeding. The genotypes of individual *AcIr76b* hetero/homozygotic mosquitoes from these assays were validated post hoc by PCR.

Capillary Feeder (CAFE) Bioassay. The CAFE bioassay was conducted following a previous study, with minor modifications (15, 44). Each trial started at ZT12 and ended at ZT18 for 6 h. Four 4- to 8-d-old mosquitoes were provided with water but otherwise fasted for 22 h before being anesthetized on ice briefly and placed into a *Drosophila* vial (24.5 × 95 mm; Thermo Fisher Scientific). A borosilicate glass capillary (1B100F-3; World Precision Instruments) was filled with 10% sucrose water and embedded into a cotton plug. The vial opening was then blocked with the cotton plug, and the capillary was placed slightly protruding from the plug into the vial for mosquitoes to feed on. The sugar level in the capillary was compared before and after each trial to generate the initial sugar consumption value. At least four control vials with no mosquitoes inside were used to assess the evaporation at the same time. The final sugar consumption was calculated by subtracting the evaporation from the initial sugar consumption value.

Results

***AcIr76b* Expression in Antennal Grooved Pegs.** In order to identify the types of antennal sensilla in which AcIr76b activity is salient, the spatial expression pattern of *AcIr76b* was established using the binary expression Q system (16, 45), which provides more sensitivity than fluorescence in-situ hybridization–based methods previously used (11). This system requires genetic crosses between a QUAS-GFP effector line and an *AcIr76b promoter-QF2* (*AcIr76b-QF2*) driver line, resulting in GFP fluorescence in *AcIr76b*-expressing cells. While previous anopheline driver lines were developed by integrating *promoter-QF2* constructs into predefined or random genomic sites (16, 45), those promoters were presumptive as they were derived from selected regions of 5′ upstream sequences without precise elucidation of the required regulatory sequences. As such, those promoters are potentially error prone and artifactual, leading to localizations that are compromised by over-/underexpression from fragmented or otherwise partial regulatory information. To overcome this limitation, we incorporated a newly developed approach using CRISPR-mediated homologous recombination to insert a *T2A-QF2-3xP3-DsRed* element into the *AcIr76b* locus at the first exon (Fig. 1*A*) (39), and the knock-in was subsequently confirmed by means of genomic PCR (Fig. 1 *A*–*C*) and sequencing. The T2A peptide induces ribosomal skipping, which facilitates the unbiased expression of *QF2* driven by endogenous, fully intact *AcIr76b* regulatory sequences (46). For localization studies, F1 progeny derived from crosses between appropriate parental driver and effector lines would therefore express the *QF2* transcriptional factor that specifically binds to the QUAS activation sequence to drive expressions of the visual marker *GFP* in all *An. coluzzii* cells that normally express *AcIr76b*.

In these studies, extensive *GFP* labeling was observed in antennal grooved pegs of 4- to 6-d-old adult female *An. coluzzii*, which would be expected to be actively seeking blood meals. Whole-mount examination of the 2nd to 13th antennal flagellomeres across multiple replicates revealed that 100% of grooved pegs, easily identified through their distinctive morphology, contained *AcIr76b*-expressing neurons displaying GFP-derived fluorescence in their dendrites (Fig. 1 *D* and *E* and *SI Appendix*, Fig. S1*A*). Moreover, these studies also identified a subpopulation of coeloconic sensilla that contain *Ir76b*-expressing neurons (Fig. 1*F* and *SI Appendix*, Fig. S1*B*). In contrast, GFP signal was never observed in any trichoid sensilla screened across more than 20 individual antennal preparations. Recent studies have uncovered noncanonical coexpression of IRs and ORs in a subset of chemosensory neurons of *Drosophila* and *Ae. aegypti* (47, 48). In that light, cryosections were prepared to investigate whether IR/OR coexpression also occurs in *An. coluzzii* by immunolocalization using Orco-specific antibodies together with *Ir76b-GFP* progeny. Our data suggest that while the majority (>95%) of *Ir76b-GFP*–positive cells were not labeled by Orco antibodies (Fig. 1*G*), a small subset did indeed coexpress both *AcIr76b* and *Orco* (Fig. 1*H*). In light of our examination of antennal trichoid sensilla as well as previous studies of *An. coluzzii* grooved pegs that indicate they are both devoid of Orco protein (10), the coexpression of *AcIr76b* and *Orco* seen here likely reflects either coeloconic or perhaps an as-yet unidentified population of sensilla.

In addition to the antennae of *An. coluzzii* females, *AcIr76b* localization analyses revealed that while the maxillary palps are devoid of *AcIr76b*-expressing cells, they are highly enriched in the labella (Fig. 1*I*) and also present on the pre, meso-, and metatarsi (*SI Appendix*, Fig. S2). On the *An. coluzzii* female labellum, *AcIr76b* is expressed in two populations of neurons with distinctive dendrites: the relatively long dendrites that innervate gustatory T1 sensilla and the short dendrites that are associated with olfactory T2 sensilla (Fig. 1*I*) (7, 49). As was the case for the antennae, *AcIr76b* and *Orco* are coexpressed in a subset of cells present on the labella of *An. coluzzii* females (Fig. 1*J*).

Generation of *AcIr76b* Null Mutants. The *AcIr76b* null mutant line was generated using the CRISPR-Cas9 system together with the DSB-specific homology template in order to knock in a *3xP3-DsRed* visible marker construct at the *AcIr76b* DSB site. The sgRNA was chosen to target the first exon of *AcIr76b* to produce an early stop codon that leads to a malfunctional protein (Fig. 2*A*). In total, 376 preblastoderm embryos were microinjected with the homologous template and the CRISPR targeting vector, in which *Cas9* expression is regulated by the *vasa2* promoter to specifically induce germ cell mutagenesis. Of the 17 larvae (4.5%) that survived the injection, two female and two male adults were able to successfully eclose and were designated as G0. These adults were then collectively crossed with the wild-type population, and the progeny (F1) were screened for the presence of red fluorescence in the eye and ventral nerve cord that would be expected if they contained a *3xP3-DsRed* insert. At least one of the G0-injected adults produced red-eyed F1 offspring,

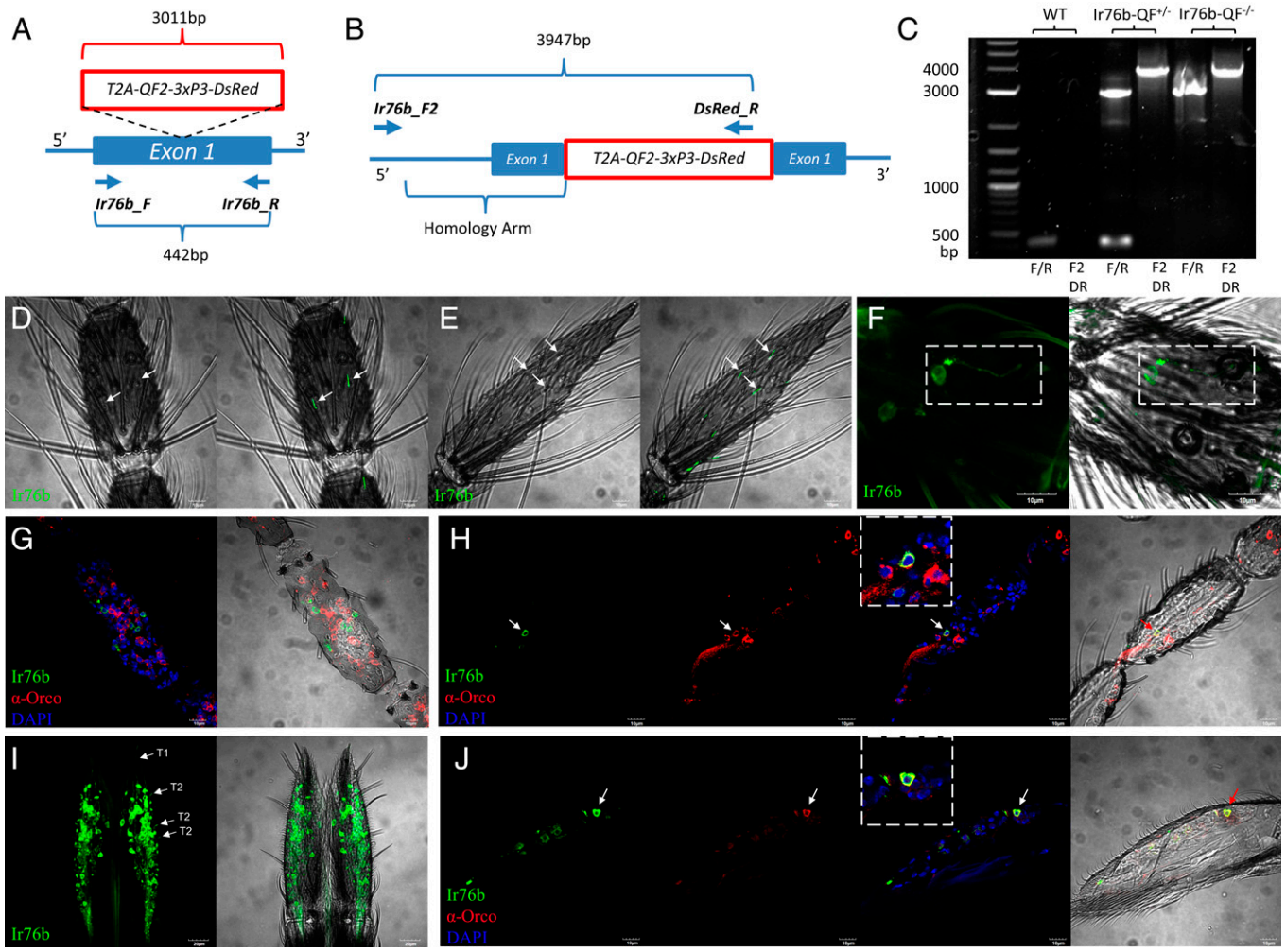

Fig. 1. Localization of *AcIr76b* in chemosensory appendages. (*A*) *AcIr76b-QF2* driver line schematics. The *T2A-QF2-3xP3-DsRed* element was inserted into the first exon of *AcIr76b* via CRISPR-mediated homologous recombination. A pair of primers (*Ir76b_F* and *Ir76b_R*) were used for genomic PCR validation. The wild type produces a 442-bp amplicon, whereas the *AcIr76b-QF2* driver allele gives rise to a 3,011-bp amplicon. (*B*) A pair of primers (*Ir76b_F2* and *DsRed_R*) were used to amplify the region outside the homology arm. The *AcIr76b-QF2* driver allele gives rise to a 3,947-bp amplicon, whereas the primers are nonspecific for the wild type. (*C*) Agarose electrophoresis of genomic PCR validation of wild type (WT), heterozygous driver (Ir76b-QF2$^{+/-}$), and homozygous driver (Ir76b-QF2$^{-/-}$) with Ir76bF/Ir76bR (F/R) and Ir76bF2/DsRedR (F2DR) primers. (*D* and *E*) Representative bright-field image (*Left*) with GFP fluorescence overlay confocal z-stacks (*Right*) of whole-mount female antennae indicating *AcIr76b* is expressed in grooved pegs on sixth flagellomere (*D*) and 13th flagellomere (*E*) (highlighted by arrows). (*F*) A representative confocal z-stack of a whole-mount female antenna showing *AcIr76b* is expressed in the cell body and dendrites of coeloconic sensilla (highlighted by dashed lines). (*G*) A representative confocal optical section of the female antennae immunohistochemically labeled with ?-Orco antisera (red) and *AcIr76b* (green), indicating that AcIr76b and Orco are localized in distinct cells. (*H*) A representative confocal optical section of a female antenna showing AcIr76b and Orco are colocalized in a cell (highlighted by an arrow and enlarged within dashed lines). (*I*) A representative confocal z-stack of a whole-mount female labellum showing *AcIr76b* is expressed in dendrites in T1 and T2 sensilla (highlighted by arrows; scale bars, 20 μm). (*J*) A representative confocal optical section of a female labellum showing AcIr76b and Orco are colocalized in a cell (highlighted by an arrow and enlarged within dashed lines). Nuclei were labeled with DAPI. Scale bars, 10 μm.

which indicates a high mutagenesis efficiency (≥25%). Red-eyed F1 males were individually back-crossed with wild-type females, after which their *AcIr76b* mutant genotype was confirmed by genomic PCR (Fig. 2 *A*–*C*) and DNA sequencing. Homozygous mutants were generated by crossing heterozygotes with progeny selected based on their high intensities of red fluorescence, and thereafter genomic PCR (Fig. 2*C*) and DNA sequencing were carried out to confirm phenotypic assessments.

EAGs Revealed Increased Responses to Amines in *AcIr76b* Mutants. In order to initially investigate the function of AcIr76b in adult antennal olfactory responses, transcuticular EAG studies were carried out to broadly compare high-concentration (10^{-1} vol/vol dilutions) responses between *AcIr76b*$^{-/-}$ and wild-type females against an odorant panel comprising acids, alcohols, aldehydes, amines, and esters. Surprisingly, in contrast to response deficits typically seen in other olfactory coreceptor mutants studies (21, 22, 30), the EAG responses to several amines, including 3-pyrroline, pyrrolidine, 3-methylpiperidine, and 1-butylamine were significantly higher in *AcIr76b*$^{-/-}$ females than wild type (Fig. 2 *D* and *E*). In addition, EAG studies failed to reveal a significant impact on responses of *AcIr76b*$^{-/-}$ females to a panel of acid stimuli (Fig. 2*E*). Comparative dose–response studies revealed that the enhanced EAG responses observed in *AcIr76b*$^{-/-}$ females were restricted to high-concentration stimulations (*SI Appendix*, Fig. S3 *A*–*F*). In addition to depolarization (downward) responses, we occasionally observed hyperpolarization potentials (upward) EAG responses to butyric acid, ammonia, and valeric acid. In total, 1/7 and 2/7 recordings from wild-type females demonstrated hyperpolarization potentials to stimulation with butyric acid and valeric acid, respectively. *AcIr76b*$^{-/-}$ females gave rise to hyperpolarizing EAG responses

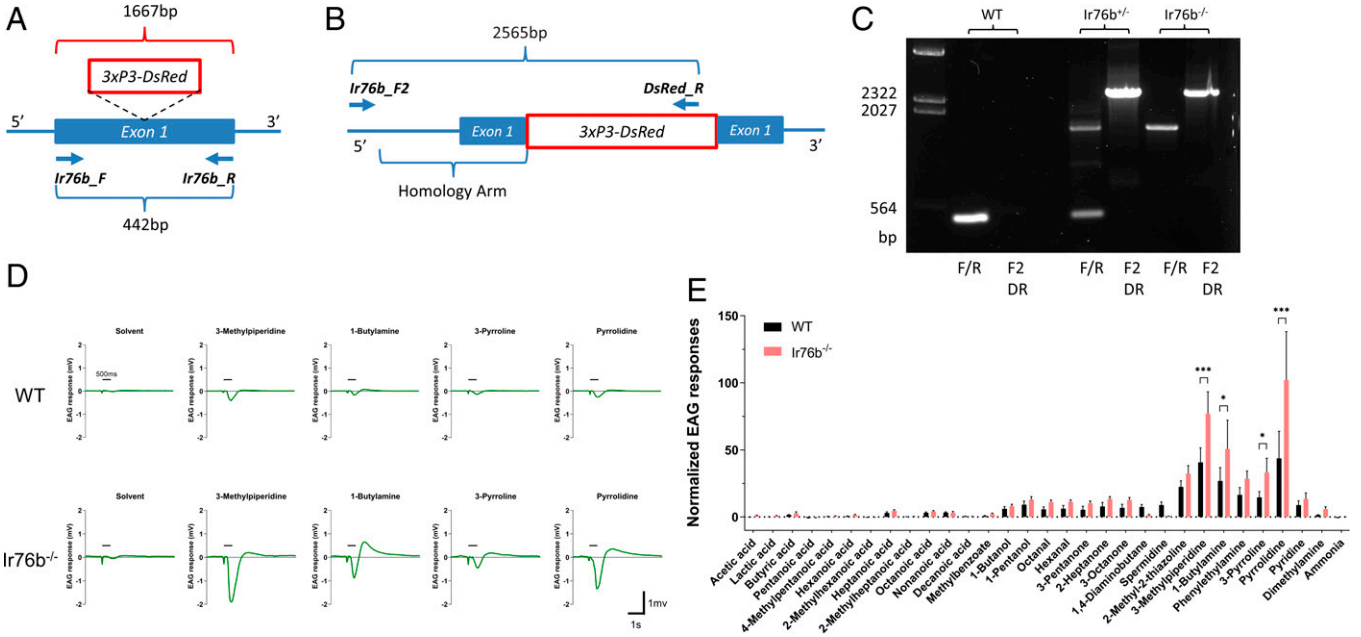

Fig. 2. EAG responses of *AcIr76b* mutants. (*A*) AcIr76b mutagenesis schematics. The *3xP3-DsRed* element was inserted into the first exon of *AcIr76b* via CRISPR-mediated homologous recombination. A pair of primers (*Ir76b_F* and *Ir76b_R*) were used for PCR validation. The wild-type genome produces a 442-bp amplicon, whereas the mutant allele gives rise to a 1,667-bp amplicon. (*B*) Primers *Ir76bF2* and *DsRedR* were used to amplify the region outside the homology arm. The *AcIr76b-QF2* driver allele gives rise to a 2,565-bp amplicon, whereas the primers are nonspecific for the wild type. (*C*) Agarose electrophoresis of genomic PCR validation of wild type (WT), heterozygotes (Ir76b$^{+/-}$), and homozygotes (Ir76b$^{-/-}$) templates using primer pairs Ir76b_F/Ir76bR (F/R) and Ir76bF2/DsRedR (F2DR). (*D*) Representative EAG recordings of wild-type (WT) and *AcIr76b*$^{-/-}$ (Ir76b$^{-/-}$) females in response to paraffin oil (solvent) and a panel of amines including 3-methylpiperidine, 1-butylamine, 3-pyrroline, and pyrrolidine. The dark bars indicate stimulus duration (0.5 s). (*E*) Averaged EAG responses to a panel of acids and amines. Multiple *t* tests (n = 5 to 7) suggest responses to amines in *AcIr76b* mutants are significantly higher than in wild type. Responses were normalized to the solvent responses. Significance levels are depicted with asterisks: P value < 0.05 (*); P value < 0.001 (***). Error bars = SEM.

to ammonia (1/7 recordings), butyric acid (2/7 recordings), and valeric acid (6/7 recordings). In any case, statistical analyses of both response profiles revealed no significant differences between the wild-type and *AcIr76b*$^{-/-}$ females to these stimuli (*SI Appendix*, Fig. S3 *G* and *H*).

Elevated Single Sensillum Responses in *AcIr76b*$^{-/-}$ Grooved Pegs. The localization of antennal *AcIr76b* suggests that the increased EAG responses to amines are most likely due to elevated neuronal responses in populations of grooved pegs. To test this hypothesis, SSR studies to characterize and compare response profiles of *AcIr76b*$^{-/-}$ and wild-type females were carried out across a randomized sampling of 14 antennal grooved pegs across the three distal-most (10th to 13th) antennal flagellomeres where the highest density (~40) of these sensilla are found (14). These data reveal a range of wild-type responses to several amines that include both excitation and inhibition (Fig. 3 *A* and *B*). Interestingly, while *AcIr76b*$^{-/-}$ mutants displayed wild-type levels of spontaneous (background) neuronal activity (Fig. 3*C*) as well as responses to pyridine, 2-methyl-2-thiazoline, and phenylethylamine, we observed significantly elevated excitation elicited by pyrrolidine, 3-pyrroline, 3-methylpiperidine, and 1-butylamine compared with the wild-type responses, with only a single group of spikes as classified by AutoSpike analysis software (Fig. 3 *A* and *B* and *SI Appendix*, Fig. S4). Furthermore, poststimulus OFF responses of grooved pegs were also analyzed, revealing significantly higher levels of neuronal spiking in the aftermath of 3-methylpiperidine stimulation in the mutants than in their wild-type counterparts (Fig. 3*D* and *SI Appendix*, Fig. S4). While increased OFF responses to pyrrolidine, 3-pyrroline, and 1-butylamine were also observed in *AcIr76b*$^{-/-}$ mutants, these differences were nonsignificant when compared to wild-type responses (Fig. 3*D* and *SI Appendix*, Fig. S4). Nonsignificant differences were also observed in the olfactory responses to amines from antennal trichoid sensilla when comparing *AcIr76b*$^{-/-}$ mutants and similarly aged wild-type female *An. coluzzii* (Fig. 3*E*).

Randomized SSR responses to acids and amines in peg-in-pit antennal coeloconic sensilla across the second to eighth flagellomeres were also carried out to explore potential *AcIr76b* function (Fig. 4*A*). While wild-type and *AcIr76b*$^{-/-}$ female coeloconic sensilla displayed similar levels of spontaneous (background) neuronal activity (Fig. 4*B*), *AcIr76b*$^{-/-}$ females became indifferent to heptanoic acid, phenylacetic acid, pyridine, pyrrolidine, 2-methyl-2-thiazoline, and 1,4-diaminobutane in contrast to robust wild-type responses (Fig. 4*C* and *SI Appendix*, Fig. S5*A*). Noticeably, acetic acid, hexanoic acid, pentanoic acid, 3-methylpiperidine, and spermidine elicited distinct, yet nonsignificant, responses between wild-type and *AcIr76b*$^{-/-}$ females (Fig. 4*C* and *SI Appendix*, Fig. S5*A*). *AcIr76b*$^{-/-}$ mutants showed decreases in poststimulus OFF responses after stimulation with pyridine and phenylacetic acid (Fig. 4*D* and *SI Appendix*, Fig. S5*B*). While *AcIr76b*$^{-/-}$ females exhibited modest, albeit nonsignificant, increases in acetic acid responses compared with wild types (*SI Appendix*, Fig. S5*A*), these mutants displayed significantly higher poststimulus OFF responses to acetic acid (*SI Appendix*, Fig. S5*B*).

Peripheral Electrophysiology Across Accessory Chemosensory Appendages. To further confirm the specificity of the antennal phenotype, we carried out SSR studies on female *An. coluzzii* maxillary palp capitate pegs (cp), which are the sole sensillar class found on that appendage (5). While previous RNA sequencing–based transcriptome profiles of the *An. coluzzii* female maxillary palps uncovered *AcIr76b* transcripts (50, 51), no GFP-labeled cells were identified on female *Ir76b-GFP* progeny, which likely reflects the sensitivity differences between

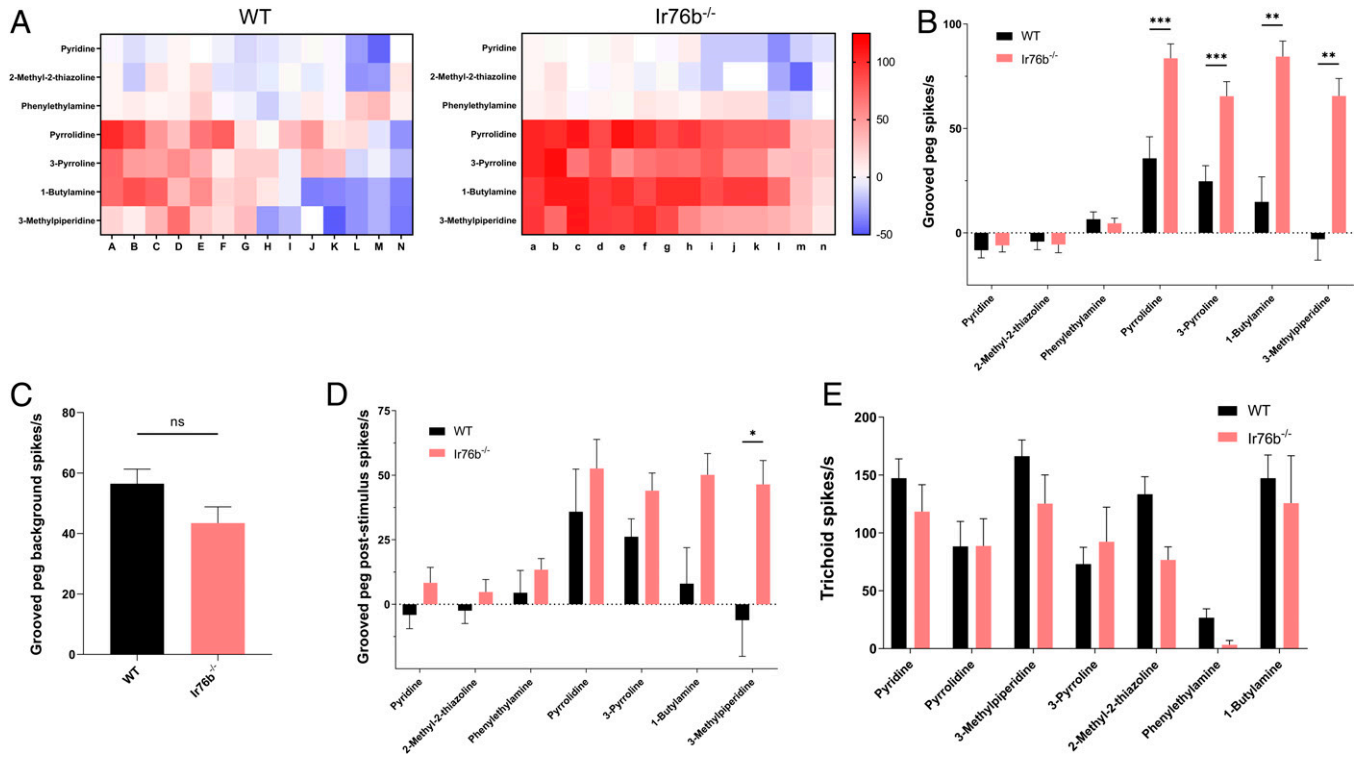

Fig. 3. SSR responses of grooved pegs and trichoid sensilla. (*A*) Heatmaps showing averaged female grooved peg SSR responses to amines in wild-type (WT) and *AcIr76b*$^{-/-}$ (Ir76b$^{-/-}$) females. Each column depicts a single replicate. The color scale marks the response amplitude from the highest (125 spikes/s, red) to the lowest (−50 spikes/s, blue). Responses were normalized by subtracting the solvent responses. (*B*) Averaged female grooved peg SSR responses. Multiple *t* tests using Holm-Sidak method ($n = 14$) suggest responses to amines in *AcIr76b* mutants are significantly higher than in wild type. (*C*) Averaged female grooved peg spontaneous (background) neuronal activity. Nonparametric *t* test suggests no significant differences between *AcIr76b* mutants and wild-type genotypes. (*D*) Averaged female grooved peg poststimulus responses. Multiple *t* tests using Holm-Sidak method ($n = 13$) suggest poststimulus OFF responses to 3-methylpiperidine in *AcIr76b* mutants are significantly higher than in wild type. (*E*) Averaged female trichoid SSR responses. Multiple *t* tests using Holm-Sidak method ($n = 6$) suggest no significant differences between *AcIr76b* mutants and wild type. Significance levels are depicted with asterisks: *P* value < 0.05 (*); *P* value < 0.01 (**); *P* value < 0.001 (***). Error bars = SEM. ns, not significant.

these two approaches. In that light, it was not surprising that the well-characterized GR- and OR-mediated responses of the cpA neuron to CO_2 and the cpB/C neurons to 1-octen-3-ol and 2,4,5-trimethylthiazole, respectively (5), were not affected in *AcIr76b*$^{-/-}$ mutants (*SI Appendix*, Fig. S6*A*).

Lastly, in light of extensive *AcIr76b* expression across the labellum (Fig. 1*G*), we also employed the ELG, an EAG-like transcuticular sampling of peripheral neuronal activity on the labellum (7), to assess responses to a panel of amines to determine whether AcIr76b might play a role in olfactory responses on that appendage. Surprisingly, in light of the robust *AcIr76b* labellum expression, these studies revealed no significant differences between the amine response profiles of the *An. coluzzii* wild-type and *AcIr76b*$^{-/-}$ female labellum (*SI Appendix*, Fig. S6*B*).

***AcIr76b* Expression in a Distinct Antennal Organ in Larvae.** *AcIr76b* expression was also examined across the larval antennae of *An. coluzzii*, which is the principal sensory appendage of this aquatic preadult life stage (41, 52). In addition to robust labeling of larval antennal neuronal cell bodies, which are clustered within the antennal shaft (*SI Appendix*, Fig. S7*A*), the *AcIr76b* promoter appears to drive GFP labeling of dendrites that specifically innervate the sensory peg organ (*SI Appendix*, Fig. S7*A*). The larval sensory peg is a distinctive uniporous apical appendage on the antennae that has been hypothesized to play gustatory roles (*SI Appendix*, Fig. S7*B*) (52, 53). *AcIr76b* localization to the larval sensory peg dendrites is distinct from the dendritic localization of *An. coluzzii* ORs to the larval sensory cone, where they are associated with olfactory signals (41, 52).

Despite their proximity at the apical tip of the larval antennae, the activity of the sensory peg is distinct from that of the OR-associated sensory cone, which acts as the primary larval olfactory organ in *Anopheles* (41, 52). While technical limitations have thus far precluded direct recording of neuronal activities from the uniporous larval peg, we nevertheless recently carried out a comprehensive electrophysiological analysis of peripheral larval sensory cone neuron responses to a wide range of volatile stimuli (41). These SSR-based methods were used to examine the functionality of wild-type and *AcIr76b*$^{-/-}$ larval sensory cones to further narrow its role to the sensory peg. As expected, based on the absence of *AcIr76b*-associated sensory cone dendrites, these recordings failed to reveal any significant differences between wild type and *AcIr76b*$^{-/-}$ mutants insofar as background neuronal activity (*SI Appendix*, Fig. S7*C*) or responses to a panel of amines (*SI Appendix*, Fig. S7*D*).

Mating and Blood-Feeding Deficits in *AcIr76b* Mutants. In addition to their impact on peripheral electrophysiology in adult females, *AcIr76*$^{-/-}$ mutants display a range of interesting behavioral and reproduction-related deficits and, as a result, cannot self-propagate under standard laboratory rearing protocols. To investigate this phenotype, we took advantage of a previously developed insemination-based mating bioassay (15) to reveal that self-mated *AcIr76b*$^{-/-}$ mutants display significantly impaired insemination rates when compared with their wild-type counterparts (Fig. 5*A*). To investigate this phenotype further, mating studies were conducted in which *AcIr76b*$^{-/-}$ females were replaced with their wild-type counterparts. Here, wild-type females successfully mated with *AcIr76b*$^{-/-}$ males to

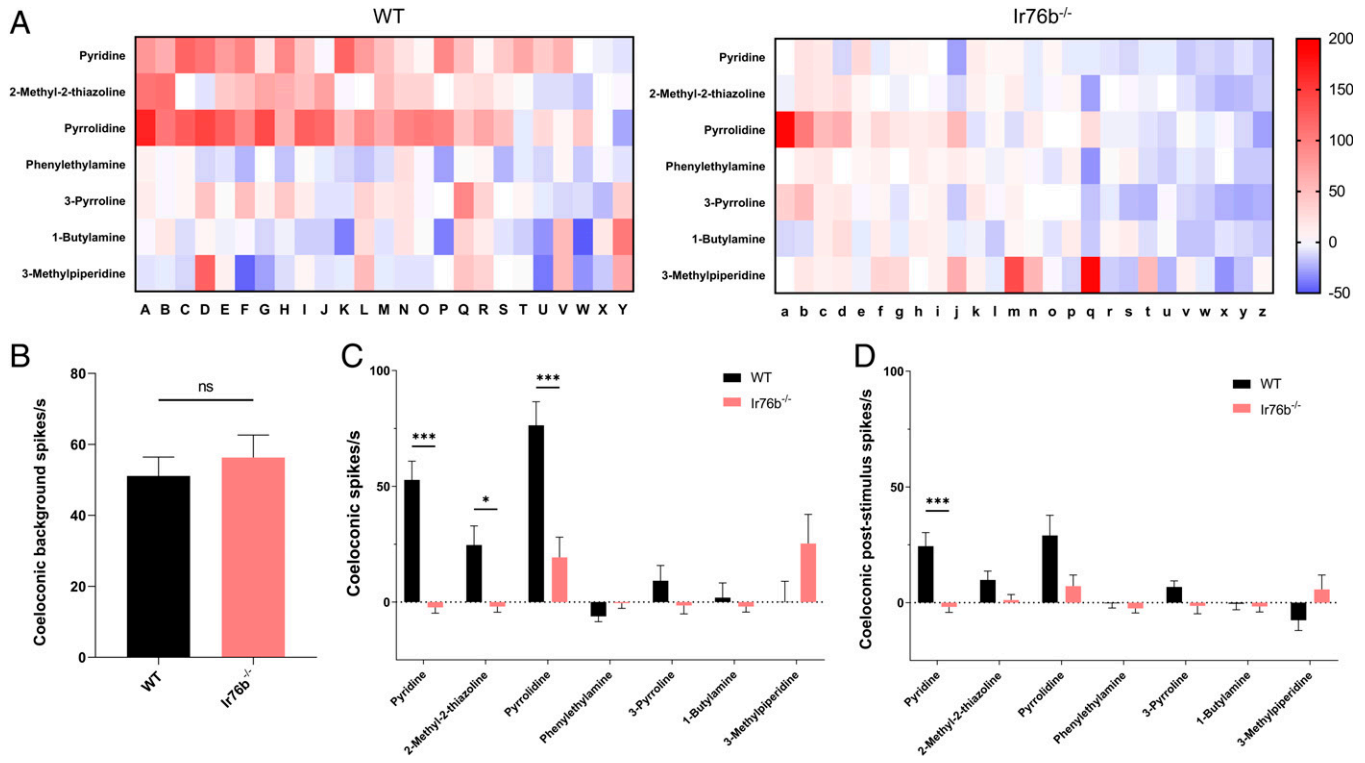

Fig. 4. SSR responses of coeloconic sensilla. (*A*) Heatmaps showing average female coeloconic sensillum SSR responses to acids and amines in wild-type (WT) and *AcIr76b*$^{-/-}$ (Ir76b$^{-/-}$) females. Each column depicts a single replicate. The color scale marks the response amplitude from the highest (200 spikes/s, red) to the lowest (−20 spikes/s, white). Responses were normalized by subtracting the solvent responses. (*B*) Averaged female coeloconic sensillar spontaneous (background) neuronal activity. Nonparametric *t* test suggests no significant differences between *AcIr76b* mutants and wild type. (*C*) Averaged female coeloconic sensillum SSR responses. Multiple *t* tests using Holm-Sidak method (n = 25 or 26) suggest responses to specific acids and amines in *AcIr76b* mutants are significantly lower than in wild type. (*D*) Averaged female coeloconic sensillar poststimulus OFF responses. Multiple *t* tests using Holm-Sidak method (n = 25 or 26) suggest poststimulus responses to acids and amines are significantly different in *AcIr76b* mutants than in wild type. Significance levels are depicted with asterisks: *P* value < 0.05 (*); *P* value < 0.001 (***). Error bars = SEM. ns, not significant.

fully rescue the mutant mating/insemination deficits. In addition, studies that paired wild-type males with *AcIr76b*$^{-/-}$ females had severe mating deficits (Fig. 5*A*), indicating that *AcIr76b* plays a female-specific role in *An. coluzzii* mating. To further investigate potential causes of these mating deficits, the gross mass of carcasses from individual females of both genotypes were compared. In these studies, *AcIr76b*$^{-/-}$ females were found to have significantly less mass than wild-type females (Fig. 5*B*), perhaps reflective of reduced fitness that, in part, might account for these mating deficits.

We next asked what other aspects of the female reproductive pathway might underlie the mating deficits and sterility of the *AcIr76b*$^{-/-}$ mutants. To address this question, we utilized a simple digital video-based blood-feeding bioassay (54) to examine whether female *AcIr76b*$^{-/-}$ mutants were able to successfully initiate and complete blood feeding. Here, 25 to 30 female mosquitoes were exposed to membrane feeders containing warmed blood meals supplemented with human foot odors released from worn socks and CO_2 for 25 min. Under these conditions, ∼30% of wild-type females successfully completed blood feeding as assessed by the presence of extended and blood-filled abdomens. We also examined alighting (landing) on the membrane feeder as a distinct component of blood-feeding behaviors by recording and quantifying those events at the surface of the blood feeder during feeding bioassays. These studies indicated that *AcIr76b*$^{-/-}$ females maintain wild-type levels of landings (Fig. 5*C*), which suggests their blood-feeding deficits are not due to the reduction of host-seeking behaviors. However, under identical conditions, while wild-type levels of alighting and probing activity were observed, none (0%) of the *AcIr76b*$^{-/-}$ females that were assayed blood fed successfully (Fig. 5*D*), even when the feeding time was extended to 2 h (120 min) with either sheep or human blood provided in the membrane feeders (Fig. 5*E*). Lastly, in light of the profound mating deficits exhibited by *AcIr76b*$^{-/-}$ females that might conceivably underlie or indirectly impact blood-feeding efficiency, we also examined the ability of virgin (unmated) wild-type females to blood feed. Here, and consistent with previous studies (55–57), wild-type virgins did not exhibit a significant alteration in blood-feeding propensity when compared with their wild-type counterparts that were first allowed to mate (Fig. 5*D*).

As is the case for other mosquitoes, *Anopheles* blood feeding is a highly specialized behavior that is quite distinct from nectar (sugar) feeding (58). Subsequent to host seeking and landing, another critical aspect of mosquito blood feeding is the process of blood ingestion (uptake), which occurs through the stylet (58). The stylet is a highly specialized component of the labellum that pierces the skin of blood-meal hosts to make direct contact with blood and is used solely for blood feeding. Recent studies in *Ae. aegypti* have illustrated the roles of *Ir7a and Ir7f*, which are expressed in stylet gustatory neurons where they are specifically responsible for mediating the direct chemosensory (taste) responses to blood-meal components (59). In light of the association of the *DmIr76b* ortholog in amino acid responses in *Drosophila* (26), we hypothesized that *AcIr76b* also acts as a gustatory IR coreceptor and, in that context, would be expressed on the stylet of *An. coluzzii*. Indeed, crosses between *AcIr76b-QF2* driver and *QUAS-GFP* effector lines revealed robust expression of *AcIr76b* in the stylet (Fig. 5*F*). In order to examine the blood-meal specificity of this feeding deficit

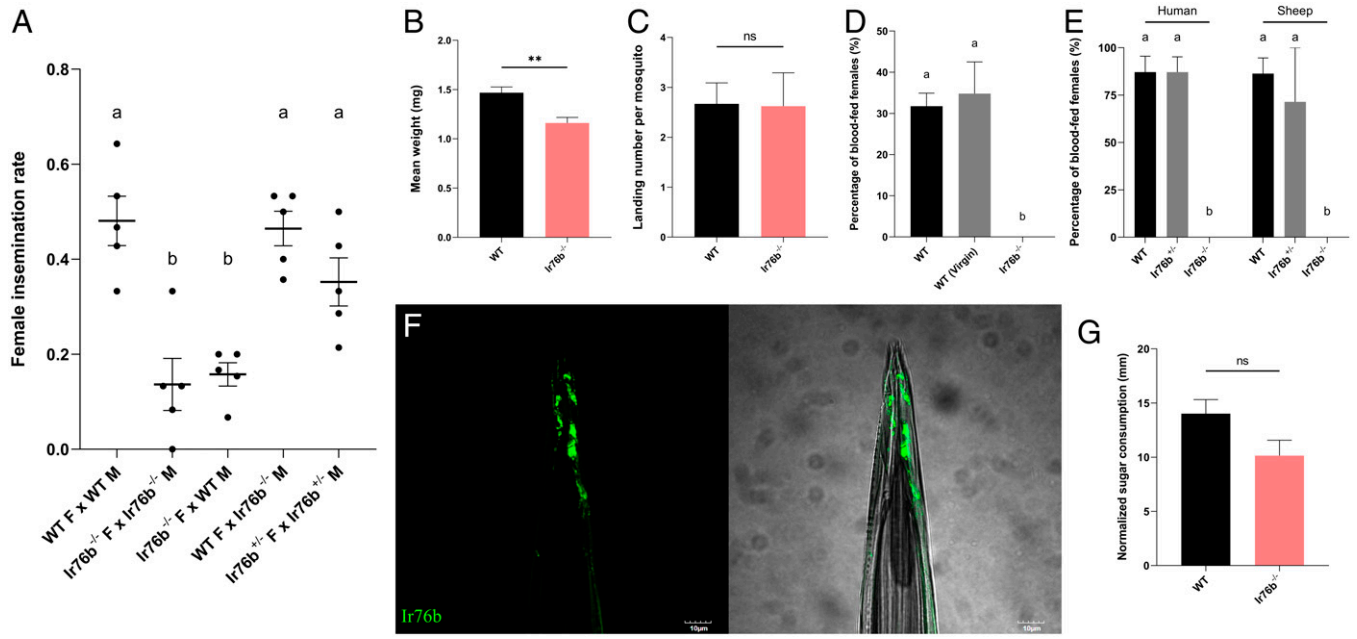

Fig. 5. Behavioral deficits of *AcIr76b* mutants. (*A*) Averaged insemination rate of females in different mating pairs. Mean values with different grouping letters were significantly different (n = 5; one-way ANOVA; P value < 0.05). (*B*) Averaged weights of the wild-type (WT) and *AcIr76b*$^{-/-}$ (Ir76b$^{-/-}$) adult females. WT females weighed significantly more than Ir76b$^{-/-}$ with P value < 0.01 (**). (*C*) Average landing counts per female mosquito on the blood feeder during blood feeding. Nonparametric t test suggests no significant differences between *AcIr76b* mutants and wild type. (*D*) Averaged blood feeding rate of wild-type (WT), virgin wild-type [WT (Virgin)], and *AcIr76b*$^{-/-}$ (Ir76b$^{-/-}$) females in a 25-min blood feeding bioassay. Mean values with different grouping letters were significantly different (n = 4 to 7; one-way ANOVA; P value < 0.05). (*E*) Averaged blood feeding rate of wild-type (WT), *AcIr76* $^{+/-}$ (Ir76b$^{+/-}$) heterozygotic, and *AcIr76b*$^{-/-}$ (Ir76b$^{-/-}$) homozygotic females in a 120-min blood feeding bioassay. Mean values with different grouping letters were significantly different (n = 5 to 7; one-way ANOVA; P value < 0.05). (*F*) A representative confocal z-stack of female stylet showing *AcIr76b* expressions. Scale bars, 10 μm. (*G*) Averaged sugar consumptions of female mosquitoes in the CAFE bioassay. Nonparametric t test suggests no significant differences between *AcIr76b* mutants and wild type. Error bars = SEM. F, female; M, male; ns, not significant.

phenotype, we used the well-established CAFE capillary feeding assay (15, 44) to examine sugar feeding. These studies confirmed *AcIr76b*$^{-/-}$ females can maintain wild-type levels of sugar feeding via their proboscis (Fig. 5*G*) that are consistent with a highly specialized blood-feeding functionality of *AcIr76b* on the stylet of *An. coluzzii*.

Discussion

Acting together or independently, anopheline IRs, GRs, and ORs are critical molecular components of the signal transduction processes that initiate diverse chemosensory processes underlying various elements of the mosquito life cycle. While many of the particulars of these relationships remain unclear, it is apparent that the collective functionality of these elements has direct implications on the biology and the vectorial capacity of these mosquitoes. Recent advances in gene-editing approaches have led to an increasingly refined appreciation of the roles of insect IR and OR coreceptors in mediating both gustatory and olfactory signal transduction, with broad implications on mosquito behavior and physiology (21, 22, 30). Here, we used state-of-the-art gene-editing/labeling approaches to characterize the expression and function of the IR coreceptor *AcIr76b* in the IR-dependent chemical ecology of the malaria vector mosquito *An. coluzzii*.

While IRs, GRs, and ORs have traditionally been presumed to populate distinct classes of chemosensory neurons, recent studies demonstrated multiple types of receptors can be coexpressed in the same neuron (47, 48). Regardless of their specific cellular context and considering the tight clustering of neurons within insect sensilla, these diverse classes of IRs may have direct as well as indirect/modulatory roles in mediating the activation or inhibition of chemosensory neurons. For example, the *Ir25a* coreceptor is coexpressed with *Gr3* and *Orco* in *Ae. aegypti* and *Drosophila*, respectively (47, 48). In *Aedes*, knocking out *Gr3* on the CO_2-sensitive cpA maxillary palp neuron removes CO_2 sensitivity but importantly does not block responses to amines mediated by *AeIr25a* in the same neurons (47). In *Drosophila*, while *Orco* null mutations completely abolished OSN activity, *DmIr25a* mutations resulted in mostly nonaltered or only partially reduced/increased responses, suggesting that *DmIr25a* plays a regulatory role when coupled with ORs instead of acting as a canonical coreceptor (48). We initially focused on the role of *AcIr76b* in adult *An. coluzzii* females that are actively host seeking for a blood meal. In these insects, robust *Ir76b* expression occurred in the antennal grooved pegs (Fig. 1), which are considered homologous to *Drosophila* coeloconic sensilla (60), as well as in T1 and T2 sensilla of the labellum (Fig. 1) and across the tarsi (*SI Appendix*, Fig. S2). We also examined its expression in the larval chemosensory system, which is housed on the antennae. Here, in contrast to the dendritic localization of *An. coluzzii* larval ORs, *AcIr76b* specifically labeled dendrites innervating the sensory peg, which is an apical uniporous structure associated with larval gustatory responses.

The availability of CRISPR-Cas9–mediated gene targeting in *An. coluzzii* allowed us to examine loss-of-function phenotypes resulting from *AcIr76b* null mutations. In addition to defective coeloconic SSR responses to amines, consistent with that observed in *Drosophila* (24), CRISPR-generated *AcIr76b* null mutants exhibited significantly enhanced antennal responses to amines in both EAG and grooved peg SSR studies in contrast to *Ae. aegypti AeIr8a* mutants that entirely abolish olfactory sensitivity to acids (30). These data are similar to previous studies that

identified enhanced gustatory responses to sugars in *Drosophila Ir76b* mutants (61) and suggest that Ir76b's modulatory function is both context dependent and evolutionarily conserved. In *An. coluzzii*, this phenotype is restricted to the large population of non–*Orco*-expressing grooved pegs, where dramatic increases in amine-elicited spike frequencies are seen in *AcIr76b* null mutants, suggesting that *AcIr76b* is responsible for inhibition of neuronal activity in those wild-type neurons. The lack of a significant alteration of other SSR spikes (*SI Appendix*, Fig. S4) suggests this is direct intraneuronal inhibition rather than indirect interaction via ephaptic coupling or other nonsynaptic effects. Furthermore, these data are also consistent with the presence of another IR coreceptor that is primarily responsible for action potential generation. This is likely to be Ir25a in light of its association with Ir76b orthologs in *Aedes* and *Drosophila* (18, 47).

Our data provide in vivo evidence for the modulatory role of *AcIr76b* in antennal responses that is specific to amines and thus extend previous studies emphasizing the role of IRs in the detection and discrimination of amines (11, 62). Importantly, many compounds in this chemical class have been identified as human emanations and are components of odor blends that robustly attract blood-feeding anopheline mosquitoes (63, 64). In contrast to exclusive gustatory functions in *Drosophila*, mosquito labella also have olfactory capabilities (7, 49). However, despite extensive *AcIr76b* expression in the labellum of female *An. coluzzii* mosquitoes, we were unable to uncover any significant electrophysiological differences to volatile odorants between wild-type and mutant mosquitoes in ELG studies. Importantly, our data do not rule out an important gustatory role for *AcIr76b* in labellum responses to contact cues such as ammonia, carboxylic and amino acids as well as other compounds present in human sweat and in blood meals themselves (65, 66). Future SSR and tip-recording studies investigating the role of labellum expression of *AcIr76b* as well as similar approaches to target the gustatory responses across the labellum and tarsi of adult *An. coluzzii*, which also express *AcIr76b*, will doubtlessly reveal functional roles.

The restriction of larval *AcIr76b* supports a direct chemosensory role of the larval peg and, moreover, is consistent with our previous RNAi-based gene-silencing studies in *An. coluzzii*, demonstrating that larval behavioral responses to aqueous butylamine are mediated by *AcIr76b* (31). While we are currently unable to physiologically examine gustatory responses of the larval sensory peg to aqueous stimuli, it is nevertheless noteworthy that $AcIr76b^{-/-}$ mutant larvae display wild-type responses to a panel of volatile odorants. Taken together, these data indicate that the AcIr76b-associated behavioral sensitivity of *An. coluzzii* larvae to aqueous butylamine and perhaps other related compounds (31) is a gustatory process mediated through the sensory peg.

Over and above the expected peripheral olfactory impacts of knocking out *AcIr76b*, we have identified novel roles for Ir76b-based signalling in anopheline reproductive pathways. To begin, female homozygotic $AcIr76b^{-/-}$ mutants displayed significant reductions in insemination rates that persisted when mated with either wild-type or mutant males. In contrast, $AcIr76b^{-/-}$ males maintained wild-type–level insemination rates when paired with wild-type females (Fig. 5*A*). While these data demonstrate this phenotype is female specific, its mechanistic basis remains unclear. While $AcIr76b^{-/-}$ females are significantly smaller than their wild-type counterparts, which may contribute to their reduced overall fitness and thereby impact mating and other behaviors, we hypothesize that the Ir76b-related mating defect is primarily linked to its impact on direct or volatile-based chemosensory processes on the labella and tarsi of *An. coluzzii*, where *AcIr76b* expression is pronounced. Indeed, *DmIr76b* is involved in multiple gustatory pathways in *Drosophila* (25, 26), where the labella and tarsi are recognized as gustatory appendages (44, 67, 68) and where multiple studies have identified IRs on those gustatory appendages that directly promote mating (67, 69, 70). While the chemosensory receptors involved in mosquito mating have not been identified molecularly, the tarsi of anopheline mosquitoes are known to be essential for mating where they presumably detect contact mating pheromones (71–73). It is therefore reasonable to suggest that mating deficits observed in $AcIr76b^{-/-}$ females could be caused by disruption of recognition pathways that are dependent on Ir76b-mediated gustatory signaling.

While mating deficits represent a significant $AcIr76b^{-/-}$ phenotype that impedes the propagation of homozygous mutant lines, the total absence of successful blood feeding of $AcIr76b^{-/-}$ females is profound, mandating heterozygotic maintenance of these lines. Despite the ability of these mutants to exhibit wild-type levels of sugar feeding and, importantly, to be fully able to locate, alight on, and even probe blood-containing membrane feeders that are supplemented with human foot-odor blends and CO_2, $AcIr76b^{-/-}$ females completely fail to take-up (ingest) blood meals. In *Ae. aegypti*, the labial stylets, which are essential for gustatory sampling (tasting) of blood, house neurons that respond to whole blood that is rich in amino acids (74) and more specifically to adenosine triphosphate, $NaHCO_3$, and NaCl (59). More importantly, while the cognate IR coreceptors responsible for these responses remain uncharacterized, two *Aedes* IRs—*Ir7a* and *Ir7f*—acting as "tuning" receptors are specifically expressed on the stylet neurons, where they directly recognize these blood-specific tastant cues to activate the uptake of blood to complete blood feeding (59). In light of the robust expression of *AcIr76b* in the stylets of adult females, it is reasonable to postulate that *AcIr76b* is the gustatory IR coreceptor that is directly involved in blood tasting in *An. coluzzii*. That $AcIr76b^{-/-}$ mutations specifically block the uptake of blood by female mosquitoes that have located, alighted on, and probed membrane feeders provides validation for this hypothesis. Inasmuch as blood feeding is paramount for *An. coluzzii* and other mosquitoes to reproduce and to acquire and transmit disease pathogens, the crucial role of *Ir76b* in blood feeding makes it a provocative target for the development of strategies to reduce mosquito vectorial capacity.

Data Availability. All study data are included in the article and/or *SI Appendix* and therefore fully accessible upon publication.

ACKNOWLEDGMENTS. We thank Zhen Li for mosquito rearing, Dr. H. Willi Honegger for critical comments, and all members of the L.J.Z. lab for suggestions. We thank the volunteer blood donor and our colleagues at the VCI for generously providing human blood. We are also very grateful to Dr. Christopher Potter (The Johns Hopkins University School of Medicine) for the generous gift of Q system mosquito lines. We thank Dr. A.M. McAinsh for scientific copyediting and acknowledge the Vanderbilt University Cell Imaging Shared Resource Core for training and use of the Olympus FV-1000 confocal microscope. This work was conducted with the support of Vanderbilt University and a grant from the NIH (NIAID, Grant No. AI127693) to L.J.Z.

Author affiliations: [a]Department of Biological Sciences, Vanderbilt University, Nashville, TN 37235

Author contributions: Z.Y., F.L., S.T.F., S.A.O., and L.J.Z. designed research; Z.Y., F.L., H.S., S.T.F., A.B., S.A.O., and L.J.Z. performed research; Z.Y., F.L., S.T.F., A.B., S.A.O., and L.J.Z. analyzed data; and Z.Y., F.L., H.S., S.T.F., A.B., S.A.O., and L.J.Z. wrote the paper.

1. M. Coetzee *et al.*, *Anopheles coluzzii* and *Anopheles amharicus*, new members of the *Anopheles gambiae* complex. *Zootaxa* **3619**, 246–274 (2013).
2. A. Molina-Cruz, M. M. Zilversmit, D. E. Neafsey, D. L. Hartl, C. Barillas-Mury, Mosquito vectors and the globalization of *Plasmodium falciparum* malaria. *Annu. Rev. Genet.* **50**, 447–465 (2016).
3. F. van Breugel, J. Riffell, A. Fairhall, M. H. Dickinson, Mosquitoes use vision to associate odor plumes with thermal targets. *Curr. Biol.* **25**, 2123–2129 (2015).
4. C. Montell, L. J. Zwiebel, Mosquito sensory systems. *Adv. Insect Phys.* **51**, 293–328 (2016).
5. T. Lu *et al.*, Odor coding in the maxillary palp of the malaria vector mosquito *Anopheles gambiae*. *Curr. Biol.* **17**, 1533–1544 (2007).
6. Y. T. Qiu, J. J. A. van Loon, W. Takken, J. Meijerink, H. M. Smid, Olfactory coding in antennal neurons of the malaria mosquito, *Anopheles gambiae*. *Chem. Senses* **31**, 845–863 (2006).
7. H. W. Kwon, T. Lu, M. Rützler, L. J. Zwiebel, Olfactory responses in a gustatory organ of the malaria vector mosquito *Anopheles gambiae*. *Proc. Natl. Acad. Sci. U.S.A.* **103**, 13526–13531 (2006).
8. F. Guidobaldi, I. J. May-Concha, P. G. Guerenstein, Morphology and physiology of the olfactory system of blood-feeding insects. *J. Physiol. Paris* **108**, 96–111 (2014).
9. S. B. McIver, Sensilla mosquitoes (Diptera: Culicidae). *J. Med. Entomol.* **19**, 489–535 (1982).
10. R. J. Pitts, A. N. Fox, L. J. Zwiebel, A highly conserved candidate chemoreceptor expressed in both olfactory and gustatory tissues in the malaria vector *Anopheles gambiae*. *Proc. Natl. Acad. Sci. U.S.A.* **101**, 5058–5063 (2004).
11. R. J. Pitts, S. L. Derryberry, Z. Zhang, L. J. Zwiebel, Variant ionotropic receptors in the malaria vector mosquito *Anopheles gambiae* tuned to amines and carboxylic acids. *Sci. Rep.* **7**, 40297 (2017).
12. G. Wang, A. F. Carey, J. R. Carlson, L. J. Zwiebel, Molecular basis of odor coding in the malaria vector mosquito *Anopheles gambiae*. *Proc. Natl. Acad. Sci. U.S.A.* **107**, 4418–4423 (2010).
13. A. F. Carey, G. Wang, C. Y. Su, L. J. Zwiebel, J. R. Carlson, Odorant reception in the malaria mosquito *Anopheles gambiae*. *Nature* **464**, 66–71 (2010).
14. R. J. Pitts, L. J. Zwiebel, Antennal sensilla of two female anopheline sibling species with differing host ranges. *Malar. J.* **5**, 26 (2006).
15. Z. Ye *et al.*, Ammonium transporter AcAmt mutagenesis uncovers reproductive and physiological defects without impacting olfactory responses to ammonia in the malaria vector mosquito *Anopheles coluzzii*. *Insect Biochem. Mol. Biol.* **134**, 103578 (2021).
16. Z. Ye *et al.*, Heterogeneous expression of the ammonium transporter AgAmt in chemosensory appendages of the malaria vector, *Anopheles gambiae*. *Insect Biochem. Mol. Biol.* **120**, 103360 (2020).
17. K. Sato *et al.*, Insect olfactory receptors are heteromeric ligand-gated ion channels. *Nature* **452**, 1002–1006 (2008).
18. R. Benton, K. S. Vannice, C. Gomez-Diaz, L. B. Vosshall, Variant ionotropic glutamate receptors as chemosensory receptors in *Drosophila*. *Cell* **136**, 149–162 (2009).
19. L. Abuin *et al.*, Functional architecture of olfactory ionotropic glutamate receptors. *Neuron* **69**, 44–60 (2011).
20. J. A. Butterwick *et al.*, Cryo-EM structure of the insect olfactory receptor Orco. *Nature* **560**, 447–452 (2018).
21. M. DeGennaro *et al.*, *orco* mutant mosquitoes lose strong preference for humans and are not repelled by volatile DEET. *Nature* **498**, 487–491 (2013).
22. H. Sun, F. Liu, Z. Ye, A. Baker, L. J. Zwiebel, Mutagenesis of the orco odorant receptor co-receptor impairs olfactory function in the malaria vector *Anopheles coluzzii*. *Insect Biochem. Mol. Biol.* **127**, 103497 (2020).
23. C. A. Yao, R. Ignell, J. R. Carlson, Chemosensory coding by neurons in the coeloconic sensilla of the *Drosophila* antenna. *J. Neurosci.* **25**, 8359–8367 (2005).
24. A. Vulpe, K. Menuz, Ir76b is a co-receptor for amine responses in *Drosophila* olfactory neurons. *Front. Cell. Neurosci.* **15**, 759238 (2021).
25. Y. V. Zhang, J. Ni, C. Montell, The molecular basis for attractive salt-taste coding in *Drosophila*. *Science* **340**, 1334–1338 (2013).
26. A. Ganguly *et al.*, A molecular and cellular context-dependent role for Ir76b in detection of amino acid taste. *Cell Rep.* **18**, 737–750 (2017).
27. L. Ni *et al.*, The ionotropic receptors IR21a and IR25a mediate cool sensing in *Drosophila*. *eLife* **5**, e13254 (2016).
28. A. Enjin *et al.*, Humidity sensing in *Drosophila*. *Curr. Biol.* **26**, 1352–1358 (2016).
29. S. Min, M. Ai, S. A. Shin, G. S. B. Suh, Dedicated olfactory neurons mediating attraction behavior to ammonia and amines in *Drosophila*. *Proc. Natl. Acad. Sci. U.S.A.* **110**, E1321–E1329 (2013).
30. J. I. Raji *et al.*, *Aedes aegypti* mosquitoes detect acidic volatiles found in human odor using the IR8a pathway. *Curr. Biol.* **29**, 1253–1262.e7 (2019).
31. C. Liu *et al.*, Distinct olfactory signaling mechanisms in the malaria vector mosquito *Anopheles gambiae*. *PLoS Biol.* **8**, 27–28 (2010).
32. C. J. Potter, B. Tasic, E. V. Russler, L. Liang, L. Luo, The Q system: A repressible binary system for transgene expression, lineage tracing, and mosaic analysis. *Cell* **141**, 536–548 (2010).
33. A. N. Fox, R. J. Pitts, H. M. Robertson, J. R. Carlson, L. J. Zwiebel, Candidate odorant receptors from the malaria vector mosquito *Anopheles gambiae* and evidence of down-regulation in response to blood feeding. *Proc. Natl. Acad. Sci. U.S.A.* **98**, 14693–14697 (2001).
34. E. Suh, D. H. Choe, A. M. Saveer, L. J. Zwiebel, Suboptimal larval habitats modulate oviposition of the malaria vector mosquito *Anopheles coluzzii*. *PLoS One* **11**, e0149800 (2016).
35. F. Liu, Z. Ye, A. Baker, H. Sun, L. J. Zwiebel, Gene editing reveals obligate and modulatory components of the CO_2 receptor complex in the malaria vector mosquito, *Anopheles coluzzii*. *Insect Biochem. Mol. Biol.* **127**, 103470 (2020).
36. A. Hammond *et al.*, A CRISPR-Cas9 gene drive system targeting female reproduction in the malaria mosquito vector *Anopheles gambiae*. *Nat. Biotechnol.* **34**, 78–83 (2016).
37. K. Labun *et al.*, CHOPCHOP v3: Expanding the CRISPR web toolbox beyond genome editing. *Nucleic Acids Res.* **47** (W1), W171–W174 (2019).
38. E. Pondeville *et al.*, Efficient ΦC31 integrase-mediated site-specific germline transformation of *Anopheles gambiae*. *Nat. Protoc.* **9**, 1698–1712 (2014).
39. B. J. Matthews, M. A. Younger, L. B. Vosshall, The ion channel *ppk301* controls freshwater egg-laying in the mosquito *Aedes aegypti*. *eLife* **8**, e43963 (2019).
40. F. Liu, L. Chen, A. G. Appel, N. Liu, Olfactory responses of the antennal trichoid sensilla to chemical repellents in the mosquito, *Culex quinquefasciatus*. *J. Insect Physiol.* **59**, 1169–1177 (2013).
41. H. Sun, F. Liu, A. Baker, L. J. Zwiebel, Neuronal odor coding in the larval sensory cone of *Anopheles coluzzii*: Complex responses from a simple system. *Cell Reports* ***36*** *(7) 109555* (2021). https://doi.org/10.1016/j.celrep.2021.109555. Accessed 17 August 2021.
42. C. J. Den Otter, M. Behan, F. W. Maes, Single cell responses in female *Pieris brassicae* (Lepidoptera: Pieridae) to plant volatiles and conspecific egg odours. *J. Insect Physiol.* **26**, 465–472 (1980).
43. R. J. Pitts, C. Liu, X. Zhou, J. C. Malpartida, L. J. Zwiebel, Odorant receptor-mediated sperm activation in disease vector mosquitoes. *Proc. Natl. Acad. Sci. U.S.A.* **111**, 2566–2571 (2014).
44. E. J. Dennis, O. V. Goldman, L. B. Vosshall, *Aedes aegypti* mosquitoes use their legs to sense DEET on contact. *Curr. Biol.* **29**, 1551–1556.e5 (2019).
45. O. Riabinina *et al.*, Organization of olfactory centres in the malaria mosquito *Anopheles gambiae*. *Nat. Commun.* **7**, 13010 (2016).
46. F. Diao, B. H. White, A novel approach for directing transgene expression in *Drosophila*: T2A-Gal4 in-frame fusion. *Genetics* **190**, 1139–1144 (2012).
47. M. A. Younger *et al.*, Non-canonical odor coding ensures unbreakable mosquito attraction to humans. *bioRxiv* (2020). https://doi.org/10.1101/2020.11.07.368720. Accessed 1 July 2021.
48. D. Task *et al.*, Chemoreceptor co-expression in *Drosophila melanogaster* olfactory neurons. eLife **11**, e72599 (2022).
49. A. M. Saveer, R. J. Pitts, S. T. Ferguson, L. J. Zwiebel, Characterization of chemosensory responses on the labellum of the malaria vector mosquito, *Anopheles coluzzii*. *Sci. Rep.* **8**, 5656 (2018).
50. R. J. Pitts, D. C. Rinker, P. L. Jones, A. Rokas, L. J. Zwiebel, Transcriptome profiling of chemosensory appendages in the malaria vector *Anopheles gambiae* reveals tissue- and sex-specific signatures of odor coding. *BMC Genomics* **12**, 271 (2011).
51. G. Athrey *et al.*, Chemosensory gene expression in olfactory organs of the anthropophilic *Anopheles coluzzii* and zoophilic *Anopheles quadriannulatus*. *BMC Genomics* **18**, 751 (2017).
52. Y. Xia *et al.*, The molecular and cellular basis of olfactory-driven behavior in *Anopheles gambiae* larvae. *Proc. Natl. Acad. Sci. U.S.A.* **105**, 6433–6438 (2008).
53. D. Nicastro, R. R. Melzer, H. Hruschka, U. Smola, Evolution of small sense organs: Sensilla on the larval antennae traced back to the origin of the Diptera. *Naturwissenschaften* **85**, 501–505 (1998).
54. C. J. McMeniman, R. A. Corfas, B. J. Matthews, S. A. Ritchie, L. B. Vosshall, Multimodal integration of carbon dioxide and other sensory cues drives mosquito attraction to humans. *Cell* **156**, 1060–1071 (2014).
55. J. D. Charlwood *et al.*, 'A mate or a meal'–Pre-gravid behaviour of female *Anopheles gambiae* from the islands of São Tomé and Príncipe, West Africa. *Malar. J.* **2**, 9 (2003).
56. T. W. Scott, W. Takken, Feeding strategies of anthropophilic mosquitoes result in increased risk of pathogen transmission. *Trends Parasitol.* **28**, 114–121 (2012).
57. C. M. Stone, I. M. Hamilton, W. A. Foster, A survival and reproduction trade-off is resolved in accordance with resource availability by virgin female mosquitoes. *Anim. Behav.* **81**, 765–774 (2011).
58. R. M. Gordon, W. H. R. Lumsden, A study of the behaviour of the mouth-parts of mosquitoes when taking up blood from living tissue; together with some observations on the ingestion of microfilariae. *Ann. Trop. Med. Parasitol.* **33**, 259–278 (1939).
59. V. Jové *et al.*, Sensory discrimination of blood and floral nectar by *Aedes aegypti* mosquitoes. *Neuron* **108**, 1163–1180.e12 (2020).
60. A. Ray, Reception of odors and repellents in mosquitoes. *Curr. Opin. Neurobiol.* **34**, 158–164 (2015).
61. H. L. Chen, U. Stern, C. H. Yang, Molecular control limiting sensitivity of sweet taste neurons in *Drosophila*. *Proc. Natl. Acad. Sci. U.S.A.* **116**, 20158–20168 (2019).
62. A. Hussain *et al.*, Ionotropic chemosensory receptors mediate the taste and smell of polyamines. *PLoS Biol.* **14**, e1002454 (2016).
63. C. K. Mweresa *et al.*, Enhancing attraction of African malaria vectors to a synthetic odor blend. *J. Chem. Ecol.* **42**, 508–516 (2016).
64. R. I. Ellin *et al.*, An apparatus for the detection and quantitation of volatile human effluents. *J. Chromatogr. A* **100**, 137–152 (1974).
65. L. B. Baker, Physiology of sweat gland function: The roles of sweating and sweat composition in human health. *Temperature* **6**, 211–259 (2019).
66. R. C. Burke, T. H. Lee, V. Buettner-Janusch, Free amino acids and water soluble peptides in stratum corneum and skin surface film in human beings. *Yale J. Biol. Med.* **38**, 355–373 (1966).
67. C. Montell, A taste of the *Drosophila* gustatory receptors. *Curr. Opin. Neurobiol.* **19**, 345–353 (2009).
68. J. T. Sparks, B. T. Vinyard, J. C. Dickens, Gustatory receptor expression in the labella and tarsi of *Aedes aegypti*. *Insect Biochem. Mol. Biol.* **43**, 1161–1171 (2013).
69. Z. He, Y. Luo, X. Shang, J. S. Sun, J. R. Carlson, Chemosensory sensilla of the *Drosophila* wing express a candidate ionotropic pheromone receptor. *PLoS Biol.* **17**, e2006619 (2019).
70. T. W. Koh *et al.*, The *Drosophila* IR20a clade of ionotropic receptors are candidate taste and pheromone receptors. *Neuron* **83**, 850–865 (2014).
71. A. Diabate, F. Tripet, Targeting male mosquito mating behaviour for malaria control. *Parasit. Vectors* **8**, 347 (2015).
72. L. S. Baik, J. R. Carlson, The mosquito taste system and disease control. *Proc. Natl. Acad. Sci. U.S.A.* **117**, 32848–32856 (2020).
73. J. D. Charlwood, M. D. R. Jones, Mating behaviour in the mosquito, *Anopheles gambiae* s.l. I. Close range and contact behaviour. *Physiol. Entomol.* **4**, 111–120 (1979).
74. A. M. Proenza, A. Palou, P. Roca, Amino acid distribution in human blood. A significant pool of amino acids is adsorbed onto blood cell membranes. *Biochem. Mol. Biol. Int.* **34**, 971–982 (1994).